Clean Technologies and Environmental Policy (2023) 25:2865–2884
https://doi.org/10.1007/s10098-023-02589-x

ORIGINAL PAPER

Strong, lightweight, thermally stable, and hydrophobic sustainable structural composites produced from coal-based waste and polymer-derived SiOC ceramics

Orevaoghene Eterigho-Ikelegbe[1] · Emmanuel Ricohermoso III[2] · Hamza Harrar[1] · Ralf Riedel[2] · Samson Bada[1]

Received: 13 March 2023 / Accepted: 12 July 2023 / Published online: 29 July 2023

Abstract
Recycling coal-based waste (CBW) into composites suitable as a building material might be a necessary response to combat its risk to the environment. Therefore, the objective of this study was to investigate the microstructure and performance of coal composites produced from CBW and polysiloxane polymer (SPR-212). Four types of CBW that differ in physicochemical properties were examined. Fourier transform infrared spectroscopy results indicated that the higher the intensity of the C=C bonds in the CBW, the higher the pyrolysis mass loss and shrinkage experienced by the composites during pyrolysis. The continuous operating temperature of the composites is up to 600 °C. However, at temperatures above 600 °C, composites containing carbon content greater than 36% manifested dramatic degradation. Pyrolysis mass loss in the range of 5.28 to 29.62% was obtained for all the composites. The density range of the composites is between 1.5 and 1.9 g per cubic centimetre. The water absorption of all the composites is within the range of 0 to 25% and is comparable to many building materials. Notably, the composites containing total carbon less than 10% registered a water contact angle greater than 90°, indicating the low wettability of their surface. Furthermore, composites that embodied the highest total carbon (63%) displayed the worst structural property. The findings of this study lay the foundation for further development of high-quality structural coal composites from CBW and the SPR-212 preceramic polymer through optimisation of the processing conditions.

✉ Orevaoghene Eterigho-Ikelegbe
1794557@students.wits.ac.za; eterighoo@gmail.com

[1] Faculty of Engineering and the Built Environment, DSI-NRF SARChI Clean Coal Technology Research Group, School of Chemical and Metallurgical Engineering, University of the Witwatersrand, Private Bag X3, Wits 2050, Johannesburg, South Africa

[2] Fachbereich Material-und Geowissenschaften, Technische Universität Darmstadt, Otto-Berndt-Straße 3, 4287 Darmstadt, Germany

Graphical abstract

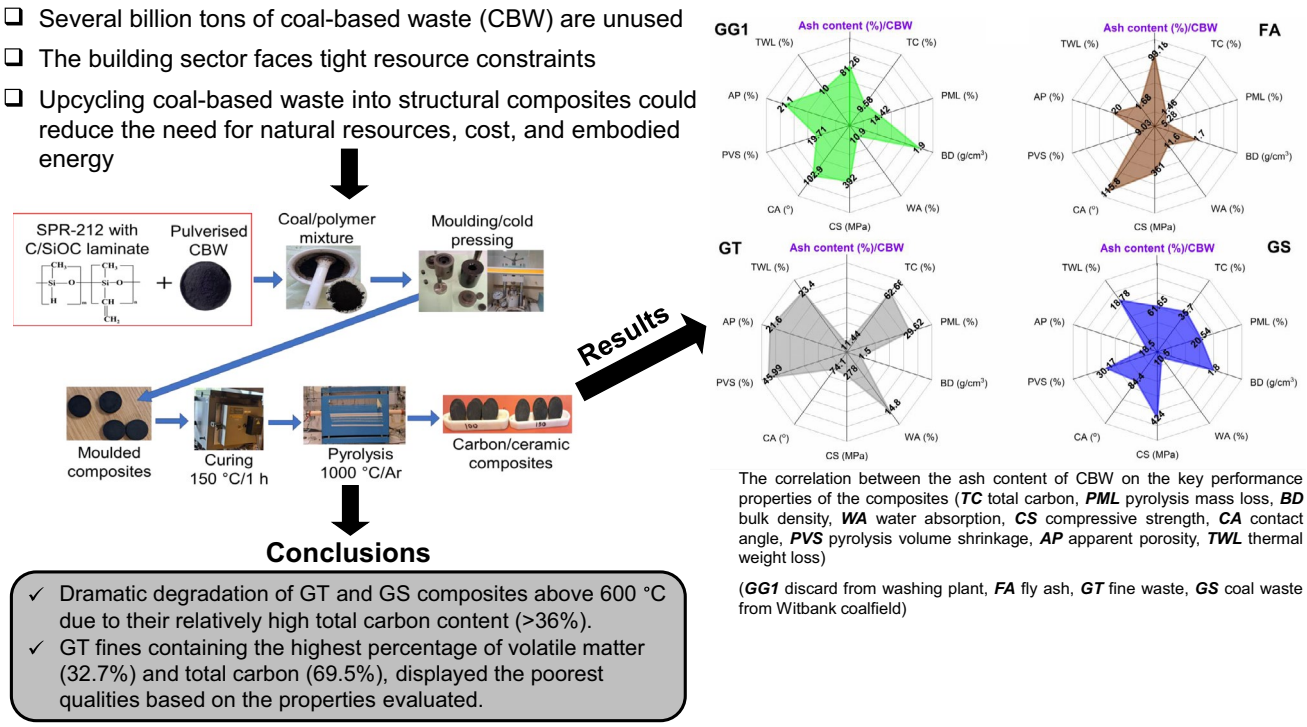

Assessment of structural composites produced from coal-based waste and polymer-derived SiOC ceramics

Keywords Building material · Carbon · Ceramics · Compressive strength · Polysiloxane · Thermal stability

Introduction

As with any mineral extraction activity, coal mining is associated with the disposal of various types of coal wastes (CW) in tailings dumps. Also, coal fly ash (CFA) represents 70-85 wt.% of the total ash generated from coal combustion in thermal power stations. As of 2012, it was estimated that about 800 million tonnes of CFA are generated worldwide annually (Blissett and Rowson 2012; Yao et al. 2014). Traditionally, CW and CFA (grouped as coal-based waste (CBW)) are diverted to landfill and have become a permanent feature around many coal mines and power stations worldwide due to their underutilisation. Undoubtedly, CBW dumps pose adverse implications on the natural environment, social well-being, and local resources (Haywood et al. 2019; Li et al. 2018; Mbedzi et al. 2020; Tambwe et al. 2020; Zhao 2012). There has been progress in the potential application of CFA and CW (Haibin and Zhenling 2010; Blissett and Rowson 2012; Yao et al. 2015; Fecko et al. 2013; Hu 2016). With a focus on circularity worldwide, a forecasted rise in CBW for much of the next 20 years, and the unused CBW available in millions of tones, developing multidimensional upcycling strategies can substantially mitigate many of its environmental burdens and enhance global industrial ecology practices. Indeed, this can be seen from the panoply of novel research solutions ongoing to generate value from CBW (Liu et al. 2018; Abdulsalam et al. 2020; Isaac and Bada 2020; Morgan and Wade 2021; Hill and Easter 2021; Eterigho-Ikelegbe et al. 2021a, b, c, 2022; Harrar et al. 2022; Hill et al. 2022). The social and environmental pressures to address concerns over waste reduction drive the incentives for CBW research. At the same time, the built environment and construction sectors are highly raw, intensive materials sectors compared to any other economic activity (Pacheco-Torgal and Labrincha 2013; Hossain et al. 2020). These sectors face increasingly tight resource constraints and a growing scarcity of good-quality raw materials due to excessive and continuous exploitation (Pacheco-Torgal and Labrincha 2013; OECD 2015). 'Resource efficiency/substitution', also known as the use of secondary resources or waste, is a current research trend to address these challenges. The goal of this approach is to promote a circular economy, preserve natural mineral resources, reduce material costs, and diminish embodied energy (Hossain et al. 2020).

One of the innovative directions of coal/CBW research is their upcycling into structural or building composites. Major research in this area include the use of coal as fillers with conventional polymers, followed by moulding (Al-Majali et al. 2019; Bai et al. 2019; Phillips et al. 2019) and firing coal/CBW in itself or mixed with clay in ceramic brick making (Stolboushkin et al. 2016; Xu et al. 2017; Vasić et al. 2021). Recently, some investigators documented a patent using US raw coal and preceramic polymer (PCP) to produce coal composites for building applications (Hill and Easter 2021; Hill et al. 2022). The formulation detail of the PCP is unknown as the information is kept proprietary. Of note, PCP, otherwise known as a ceramic-forming polymer, is a special type of polymer precursor that offers simple and inexpensive access to various ceramic systems known as polymer-derived ceramics (PDCs). The PDCs are achieved through a controlled heating process of crosslinking and pyrolysis under an inert or reactive atmosphere. These ceramic-forming polymers are used to produce advanced/technical ceramics, ceramic fibres/matrix composites, monolithic bodies, foams, coatings, membranes, and microelectromechanical systems (MEMS) (e.g. microreactors and microsensors) (Liew et al. 2000; Colombo et al. 2010; Eckel et al. 2016; Wen et al. 2022). The remarkable properties of PDCs stem from the unique combination of their inherent covalent (polar) Si-O-Si bonds and amorphous nature (Ionescu et al. 2012; Černý et al. 2015).

The manufacturing process of the patented coal composites involves curing the coal/PCP mixture followed by pyrolysis treatment (Hill and Easter 2021; Sherwood et al. 2021; Hill et al. 2022). Several attributes of the composites include lightweight, adequate strength, thermal stability, fire resistance, etc. These attributes make them suitable for application in the construction industry as roofing tiles, bricks, panels, and blocks. According to the investigators, high volatile matter coals produced composites that were inferior compared to the lower volatile matter coals. The interesting result achieved by Hill and Easter (2021) using the run-of-mine thermal coal for power generation inspired the investigation of South African high-ash coal waste with the same proprietary polymer (Eterigho-Ikelegbe et al. 2021b, 2022). The characterisation of the microstructural and physicomechanical properties of the produced composites has been documented.

For this study, different South African CBW were investigated to explore the potential of this approach further and to divert them from landfills. As suggested by Hill and Easter (2021), other PCPs capable of being pyrolysed to form ceramic may be selected or tested. Within this context, it becomes necessary to broaden the research using a commercial PCP as the ceramic binder. It is known that the physicochemical properties of CBW vary according to its origin and the seam from where the coal is mined. As such, CBW selection becomes an important factor when considering commercial PCP. Many poly(organosiloxanes) (PSOs) have excellent hydrophobic properties, act as water-repellent coatings, and are used in construction as sealants and electro-insulating agents (Greil 1995; Gumula et al. 2009; Colombo et al. 2010). PSOs are available in high volumes and easily accessible, show excellent physicochemical properties, have a long storage life, are low cost, and are easy to handle under ambient conditions (Greil 1995; Colombo et al. 2010; Černý et al. 2015). Based on these attributes, SPR-212, a commercial SiOC-yielding PCP under the class of PSOs, was considered the ceramic-forming binder for this study. Fourier transform infrared spectroscopy with attenuated total reflectance (FTIR-ATR) was employed to assess the chemical composition of the raw materials and the pyrolysed composites. X-ray diffraction (XRD), scanning electron microscopic (SEM), and Raman spectroscopy were used to provide information on the mineral composition, microstructure, and carbon phases of the composites. Thermogravimetric analysis (TGA) was used to evaluate the thermal stability/ continuous operating temperature of the composites. The density, water absorption, and apparent porosity of the composites were calculated following ASTM C67 and C373 standards. The surface property of the composites was evaluated using water contact angle measurement while their mechanical performance was studied using compression strength tests.

Experimental and characterisation

Materials and preparation of the composites

The coal-based waste (CBW) used for this study, i.e. GT, GG1, and GS were sourced from different collieries in South Africa. GT is a fine from the mined semi-soft coking coal while GG1 is a discard from the washing plant, both from the Waterberg coalfield. GS was collected from the Witbank coalfield and fly ash (FA) was obtained from one of Eskom's coal-fired power stations in the Witbank region. Commercially available low-viscous methylvinylhydrogen polysiloxane (Polyramic® SPR-212 from Starfire Systems Ltd., USA), with a 17 wt.% carbon content, was used as the ceramic-forming binder for the coal matrix. As shown in the inset of Fig. 1, the polysiloxane contains monomethylsilane and methylvinylsilane units in the Si-O-Si backbone of the polymer. The polymer was used without solvent or catalyst. The as-received size of GT, GG1, and GS samples from the mines was around -212 µm. These samples were then sent to an external laboratory where it was milled to -106 µm according to ISO 13909 standard (ISO 13909-1: 2016) for coal sampling. FA was used in the as-received state without

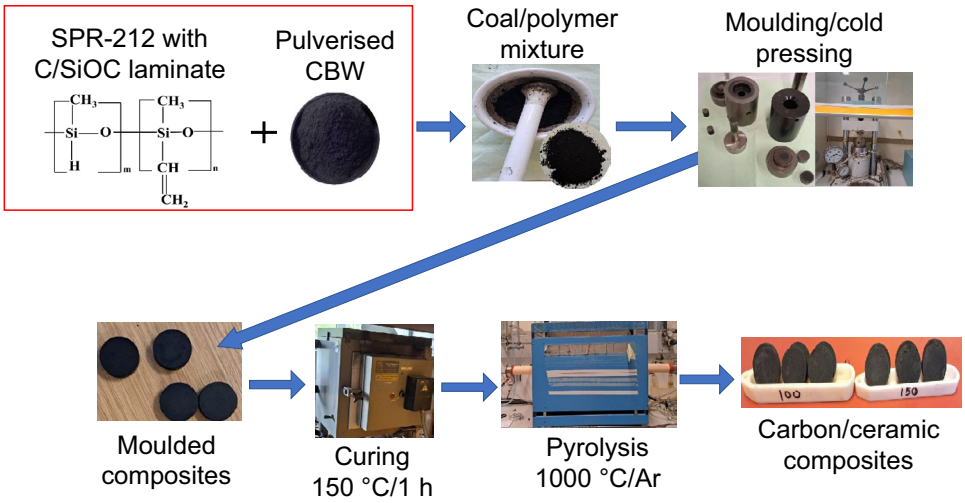

Fig. 1 Preparation of the composites

Table 1 Particle size distribution and textural properties of the CBW samples

Property	GG1	FA	GT	GS
PSD D10, µm	38.92	10.05	20.30	0.28
PSD D50, µm	87.07	35.56	58.79	11.22
PSD D90, µm	99.82	55.63	70.29	43.52
MBET, m^2/g	9.89	1.29	3.05	3.61
TPV, 10^{-2} cc/g	3.09	0.47	1.76	1.14

GG1 discard from washing plant, *FA* fly ash, *GT* fine waste, *GS* coal waste from Witbank coalfield, *PSD* particle size distribution, *MBET* multi-point BET surface area measured by nitrogen adsorption, *TPV* total pore volume, *D10 µm* 10% of GG1 sample has a size of 38.92 µm or smaller

any pre-treatment. About 60% of the particle size distribution of the CBW is under -82 µm. The particle size distribution and textural property results of the CBW are presented in Table 1. The preparation of the composites was based on method adopted from the literature (Hill and Easter 2021; Sherwood et al. 2021; Hill et al. 2022). In this study, a ratio of CBW to SPR-212 of 80:20 weight per cent was poured into a porcelain mortar and properly hand-mixed for about five minutes with a pestle until homogeneity was achieved. About 1.93 g of the resultant mixture was evenly distributed into a die and compacted using a manual press of applied force, 8 to 10 kilonewtons for about 30 s before release to produce circular composites. For the CBW particles to be well laminated by the precursor and to maintain structural integrity during pyrolysis, thermal crosslinking was initiated. The shaped bodies placed in alumina crucibles were heated in an airtight furnace with a ramp rate of 5 °C/min up to 150 °C (below the degradation temperature of the CBW and PCP) and held for one hour. Finally, the resulting cured bodies were pyrolysed in a sealed alumina tube furnace at a rate of 100 °C/h (1.67 °C/min) under flowing argon to 1000 °C and held isothermally for ten hours. After pyrolysis, the furnace was allowed to cool naturally to room temperature at 150 °C/h. Figure 1 demonstrates the summary of the production process of the composites.

Physicochemical and microstructural characterisation of the coal-based wastes and composites

Physicochemical analysis was conducted to acquire an understanding of the physical and chemical variation of coal-based waste (CBW). Proximate and ultimate analysis of the CBW was conducted following ASTM D5142 (ASTM D5142, 2009) and ISO 12902-CHN standard (ISO/TS 12902, 2001), respectively. The elemental composition of the composites was determined using a Flash 2000 CHNS elemental analyser (Thermofisher Scientific). Attenuated total reflectance-FTIR spectroscopy (Spectrum Two™ spectrometer from PerkinElmer) was used to identify the various functional groups in the CBW and composites. Fine samples were scanned in the transmission mode from 400 to 4000 cm^{-1} at a step size of 4 cm^{-1}. XRD patterns were obtained using the D2 phaser equipment (Bruker Corporation, Germany) containing an X-ray generator operating at 30 kilovolts and 10 milliamperes with a copper tube radiation (wavelength = 1.54184 Å). The analysis was conducted using a step size of 0.01° and a dwell time of ten seconds per step with a range of diffraction angle from 2-theta of 10 to 90°. The mineralogical phases in the CBW and composites were qualitatively identified using the PANalytical X'Pert software. Surface morphologies of carbon-coated composites were obtained using a scanning electron microscope (Sigma 300 VP, ZEISS, Germany). Energy-dispersive X-ray spectroscopy was used to estimate the semi-quantitative chemical compositions of the composites. The Olympus BX41 fluorescence microscope provided additional information on the microstructure of the composites' surface.

The degree of graphitisation of the carbon phase of fine composite ceramics was investigated with a Raman spectrometer (LabRAM HR fitted with an Olympus BX41 microscope and a 514.5 nm laser excitation source of the Lexel Model-95 SHG argon-ion laser). A thermogravimetric analyser (TGA701, LECO Corp., USA) was used to determine the continuous operating temperature of the composites. Approximately one gram of broken pieces of the composites was placed under an air and oxygen atmosphere in the temperature range of 25-900 °C and at a ramp rate of 10 °C/min.

Physicomechanical and surface properties of the composites

The properties and performance of the pyrolysed composites were investigated based on their bulk density, firing shrinkage, water absorption, and compression strength. The pyrolysis mass loss, radial shrinkage, and volume shrinkage experienced by the cured composites upon pyrolysis were determined by measuring the dimensions of the pyrolysed products before and after pyrolysis using Eqs. 1 to 3. Five composites were measured using a sliding gauge, and the average value was used to represent the total shrinkage and pyrolysis mass loss to the nearest 0.01%.

$$\mathrm{PML} = \frac{M_\mathrm{P} - M_\mathrm{C}}{M_\mathrm{c}} \times 100 \tag{1}$$

$$\mathrm{RS} = \frac{L_\mathrm{p} - L_\mathrm{C}}{L_\mathrm{c}} \times 100 \tag{2}$$

$$\mathrm{VS} = \frac{V_\mathrm{p} - V_\mathrm{C}}{V_\mathrm{c}} \times 100 \tag{3}$$

where PML is the pyrolysis mass loss (%), RS is the radial shrinkage (%), VS is the volume shrinkage (%), M_c is the cured mass of the composite (g), M_p is the pyrolysed mass of the composite (g), L_c is the cured length of the composite (mm) and L_p is the pyrolysed length of the composite (mm).

Water absorption, bulk density, apparent porosity, and apparent specific gravity were computed with guidance from ASTM C67 (ASTM C67, 2010) and C373 (ASTM C373, 2018) standards and following Eterigho-Ikelegbe et al. (2021b). The uniaxial compressive stress performance of the composites was tested using a benchtop universal testing machine (H100K-S) with a capacity of 10 Tonnes and guidance from ASTM C67 (ASTM C67, 2010) standard. The composite was placed flatwise between two steel loading platens to minimise machine wear. The load was applied continuously at a steady rate of 1 mm/min up to failure. The ultimate compressive stress was automatically generated using Eq. 4.

$$C = \frac{W}{A} \tag{4}$$

where C is the ultimate compressive stress to the nearest 0.01 MPa, W is the maximum load indicated by the testing machine (Kgf or N) and A is the average gross area of the upper and lower surfaces of the composite (mm^2).

The wetting behaviour/surface property of the composites was investigated based on the static contact angle (CA) measurement. An OCA 15EC goniometer (DataPhysics Instruments, GmbH, Germany) was used for this investigation. The composite surface was dosed with a droplet of water (dosing volume = 3 µL; dosing rate = 2 µL/s) at room temperature for ten seconds. The average water CA was recorded after taking at least seven readings at different spots on both surfaces of the composites.

Results and discussion

Physicochemical assessment of the coal-based waste and coal composite

The physicochemical property of the coal-based waste (CBW) in terms of proximate and elemental compositions is summarised in Table 2. The CBW reveal substantial differences regarding their volatile matter, fixed carbon, ash

Table 2 Physicochemical composition of the coal-based wastes (wt.%, air-dried basis)

Sample ID	Proximate analysis				Elemental composition					Atomic ratio	
	M	VM	A	FC*	TC	H	O*	N	TS	H/C	O/C
GG1	3.28	10.01	81.26	5.44	7.50	1.06	5.46	1.44	–	1.68	0.55
FA	0.14	0.47	99.18	0.22	–	–	–	–	–	–	–
GT	3.84	32.7	11.44	52.06	69.5	4.90	7.97	1.41	0.94	0.84	0.09
GS	1.71	20.37	61.65	16.27	23.77	1.74	8.02	0.63	2.48	0.87	0.25

GG1 discard from washing plant, *FA* fly ash, *GT* fine waste, *GS* coal waste from Witbank coalfield, *A* ash content, *FC* fixed carbon, *M* inherent moisture, *TC* total carbon, *TS* total sulphur, *VM* volatile matter

*Oxygen by calculation = [100-(M + A + carbon + hydrogen + nitrogen + sulphur)]; *FC by calculation = [100-(VM + A + M)])

Table 3 Elemental composition of the pyrolysed composites

Sample ID	TC	H	N	TS	O + Si
GG1	9.58	0.32	0.17	0.64	89.29
FA	1.46	0.26	0.07	0.28	97.93
GT	62.66	0.65	0.80	0.36	35.58
GS	35.7	0.48	0.38	1.86	61.58

TC total carbon, *H* hydrogen, *N* nitrogen, *TS* total sulphur, *O* oxygen, *Si* silicon

content, and total carbon. GT, being a semi-soft coking coal fine, manifested the lowest ash content, and the highest fixed carbon and total carbon. The hydrogen/carbon (H/C) atomic ratios of GG1 (1.68) and GS (0.87) suggest it contains a high proportion of aliphatic chains. In addition, GG1 has a high chance of forming hydrogen bonds with the PCP and it is beneficial for this type of application (Hu et al. 2017; Eterigho-Ikelegbe et al. 2021c). GG1 also has the highest oxygen/carbon (O/C) atomic ratio, implying that it is an oxidised coal rich in oxygen-containing functional groups (carboxyl, carbonyl, ether, and hydroxyl). These groups impart GG1 with good chemical reactivity (Wang and Zhou 2011; Tan et al. 2019; Eterigho-Ikelegbe et al. 2021c). The total carbon of the GT composite (63%) from Table 3 suggests that a good proportion of its mass contains carbonaceous materials after pyrolysis. The oxygen + silicon fraction in Table 3 assumes that no other elements are present in the composites other than the ones listed.

Microstructural analysis of the coal-based wastes and coal composites

Fourier transform infrared spectra

FTIR spectroscopy was used to determine the functional group composition of the CBW, the SPR-212 polymer, and the resultant composites. FTIR spectroscopy was also useful in probing the chemical interactions that occurred during the pyrolysis of the blend of coal and the SPR-212 polymer. The main functional groups of the SPR-212 resin (Xifan 2019) are shown in the FTIR spectrum of the liquid displayed on an absorbance scale (Fig. 2). The SPR-212 contains silicon-bonded hydrocarbon constituents, including methyl (CH_3) and vinyl groups (-CH=CH_2), hydride (Si-H) functionality, Si-O (backbone), and Si-C bond structures. The FTIR spectra of CBW and the resultant composites are compared in Fig. 3. The summary of functional groups detected in the CBW and coal composites is listed in Table 4. The assignment and identification of various functional groups in coal were referenced to work presented in the literature (van Niekerk, 2008; Ferraro and Basile 2012; van der Merwe et al. 2014). Only GT fines feature the aliphatic C-H stretch

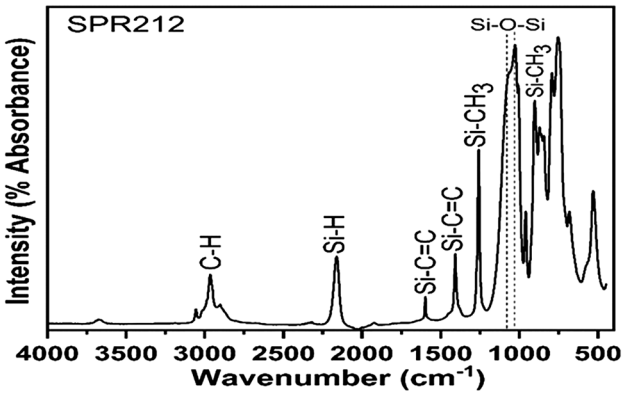

Fig. 2 Fourier transform infrared spectrum of the native polysiloxane SPR-212

(f_2) spotted between 2197 and 2852 cm^{-1}. FA, a by-product of coal combustion from a power-generating plant, did not feature the main bands normally found in coal.

From the literature (Hill and Easter 2021; Sherwood et al. 2021), moisture, low temperature/light volatile molecular species, and hydrocarbon are released creating nanopores within the coal particles and/or coal-PCP interface between 5 and 450 °C. Hence, the bands around 3700 to 3500 cm^{-1} (s_1) assigned to the O-H stretching vibrations of the mineral matter in the coal declined in the composites (p_1). Absorption bands (s_2) observed between 3000 and 2800 cm^{-1} as a result of the aliphatic C-H moieties in coal were more intense in the composites (p_2, p_3). The disappearance of the Si-vinyl (Si-C=C), Si-hydride (Si-H), and methyl silyl (Si-CH_3) peaks in the polymer suggest that these bonds broke down during pyrolysis. The redistribution reactions between these bonds with that of the coal resulted in increased absorbance of the aliphatic structural groups (alky C-H) denoted by p_2, p_3, p_4, and p_5. The C-H band is most absorbed in the FA composite and can be linked to an increase in aliphatic molecules emanating from the PCP pyrolysis.

The aromatic C=C bands in coal at about 1600 cm^{-1} (GT > GS > GG1 > FA) in terms of absorbance) are heat resistant between 50 and 450 °C (Khare and Baruah 2014). At the same time, the single bonds in the PCP (Si-H, C-H, and Si-C) and in the coal generate various hydrocarbon radical intermediates (Sharma 2018) that nucleate on bonding substrates. It is believed that the intense degradation of the aromatic C=C bonds occurred between 450 and 800 °C with the corresponding evolution of relatively high molecular weight species (devolatilisation). Above 400 °C, the PCP starts transforming to ceramic through the cracking of the Si-C bonds (Černý et al. 2015). According to Taha et al. (2017), the destruction of the double bonds in coal suggests the decomposition of organic matter. As pyrolysis progresses, some of the dissociated bonds recombine with the macromolecular fragments generated during pyrolysis to

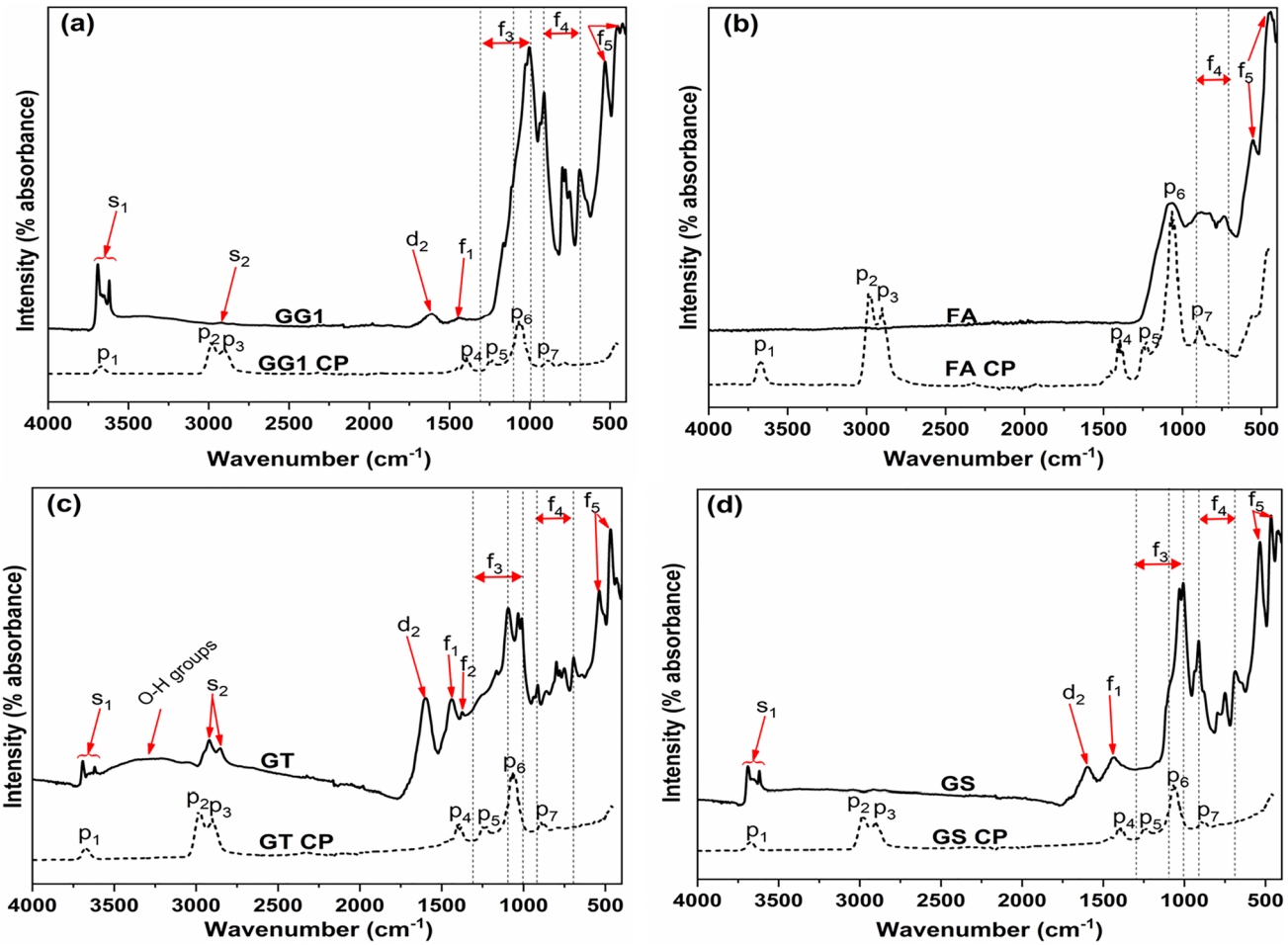

Fig. 3 Fourier Transform Infrared spectra of the CBW and their corresponding composites (*GG1* discard from washing plant, *FA* fly ash, *GT* fine waste, *GS* coal waste from Witbank coalfield)

form new bonds (resolidification). Subsequently, minerals such as kaolinite undergo dihydroxylation to form metakaolin (amorphous kaolinite) and pyrite decomposes into elemental iron and sulphur (O'Gorman and Walker 1973; Hill and Easter 2021). Apart from the contribution of weight loss that occurred during the polymer transformation to ceramic, the decomposition of the C=C bonds in coal was directly linked to the pyrolysis mass loss and shrinkage experienced by the composites. It was observed that the higher the intensity of this bond, the higher the mass loss and shrinkage of the composites, as discussed in Sect. "Weight loss and shrinkage during pyrolysis".

Above 800 °C, amorphous kaolinite decomposes into nanosized silica (silicon dioxide) and alumina (aluminium oxide) and to amorphous mullite (not detected by XRD). These nanosized products then merge to domains of graphitised carbon and are chemically bound into a ceramic structure through Si-O-Si bonds formed by the transformation of the PCP into ceramic (Solomon 1981; Hill and Easter 2021). Referring also to the FTIR spectra presented in Fig. 3, the f_3 peaks of the coals have transformed to p_6 in the composites. The disappearance of f_4 peaks in the coals assigned to the aromatic C-H vibrations reflects a substitution reaction that had taken place during pyrolysis. The fingerprint region of the CBW (f_3-f_5), in general, underwent extensive rearrangement transforming to a dominant band centred around 1065 cm^{-1} (p_6) in the composites. This band has been assigned to the -Si-O- stretching vibration associated with quartz and Si-O-Si bonds in ceramics (Gumula et al. 2009), while the weak peaks below 1000 cm^{-1} observed in the composites were ascribed to quartz and Si-C vibrations (Gumula et al. 2009; Taha et al. 2017).

X-ray diffraction analysis

X-ray diffraction was utilised to investigate the mineral phase rearrangement after pyrolysis treatments (Fig. 4). The absence of an amorphous hump suggests that the FA does not contain the aluminosilicate glass phase. Mineralogically, the association of crystalline quartz (silicon dioxide) and

Table 4 Summary of the various functional groups within the coal structure

Wave number (cm^{-1})	Peak/Vibration	Band assignment/functional groups
3690 to 3618	s_1	O-H stretching vibrations relating to kaolinite, mineral matter (surface and inner surface -OH groups)
2917 to 2852	s_2	Aliphatic C-H stretch
2917		Asymmetric CH_2 vibrations
2852		Symmetric CH_2 and CH_3 vibrations
1598	d_2	Aromatic C=C stretching vibrations
1440	f_1	CH_2, CH_3 bending vibrations
1368	f_2	CH_3 groups
1300 to1000	f_3	C-O stretch, C-C stretch, and O-H bending vibrations, alcohols, phenols, ethers, phenoxies and esters
911 to 684	f_4	Si-O-Si asymmetric stretching vibrations and Al-O-Al symmetric stretching vibrations associated with aluminates and silicates; out-of-plane aromatic C-H bend
< 700	f_5	O-Si-O symmetric bending vibrations/deformations associated with aluminates and silicates; Al-O-Al stretching vibrations associated with minerals; S-S vibrations associated with pyrite
Composites		
3700 to 3600	p_1	O-H stretching vibrations
3000 to 2900	p_2/p_3	Alkyl C-H stretching vibration
1395	p_4	C-H stretching vibration
1229	p_5	C-H stretching vibration
1055	p_6	Si-O-Si asymmetric stretching vibration
879	p_7	quartz vibrations

mullite phases is mainly visible in the FA waste. Mullite is an aluminosilicate mineral formed from the decomposition and transformation of kaolinite (a clay mineral) at elevated temperatures (Xu et al. 2017; Rautenbach et al. 2020). Quartz, anorthite, and hematite mineral phases were detected in the FA composites. The anorthite (calcium aluminosilicate) mineral phase is usually formed by the reaction of mullite and the transformed product of lime (calcium oxide). The detection of anorthite suggests that minor impurities like calcium oxide might be present in the FA (Yuan et al. 2022). Further work is needed to fully characterise the oxides in the coal using X-ray fluorescence analysis. Microcline, a potassium-rich alkali feldspar was detected in GS coal while the kaolinite phase is well present in GG1, GS, and GT. The basic unit of the kaolinite mineral consists of a tetrahedral sheet of silicon dioxide siloxane units and an octahedral sheet of aluminium hydroxide (Zhang et al. 2017). Referring to the mineralogical composition of GG1, GS, and GT composites, the results show that the kaolinite mineral phases in these coals have disappeared. Ideally, kaolinite decomposes at around 700 °C through a process of dihydroxylation (Rautenbach et al. 2020) to form quartz. Besides, some quartz still exists in these composites but in a different phase because at 570 °C quartz undergoes quartz inversion (O'Gorman and Walker 1973; Wang and Zhou 2011). Furthermore, quartz is a refractory mineral and is usually non-reactive depending on the mineral association. The new mineral phase rutile (titanium dioxide) detected in the GG1 composite can be attributed to the dissolution reaction of quartz in the presence of kaolinite during pyrolysis. The presence of a broad hump centred at a 2θ-theta value of approximately 10° typical of amorphous carbon or carbonaceous matter (Song et al. 2011) is observed in the diffractogram of GT coal and the GT composite. As stated earlier, GT is a high-rank coal (semi-soft coking coal fines); hence, some graphite crystallite peaks were detected as a result of pyrolysis up to 1000 °C.

Scanning electron and optical imaging

Scanning electron microscopy-backscattered electron (SEM-BSE) and energy-dispersive spectroscopy (EDS) analysis was used to observe the surface morphologies and elemental differences of the composites. SEM-BSE images of the carbon-coated composites presented in Fig. 5 show some cracks on the surface of the composites. These cracks could have been caused by thermal stresses and shrinkage experienced by the composites during pyrolysis. It could also be possible that the cracks were formed when breaking a small composite sample for SEM imaging. The area energy-dispersive spectroscopy of the composite surface shows the stoichiometry of the detected elements. The FA composite contains traces of carbon and anorthite grains associated with quartz. In addition, quartz, representing the most abundant phases, seems to be bonded by a carbon matrix formed from the pyrolysis of the PCP. SEM imaging of the GT composite revealed grains of phosphate minerals (monetite). The surface of

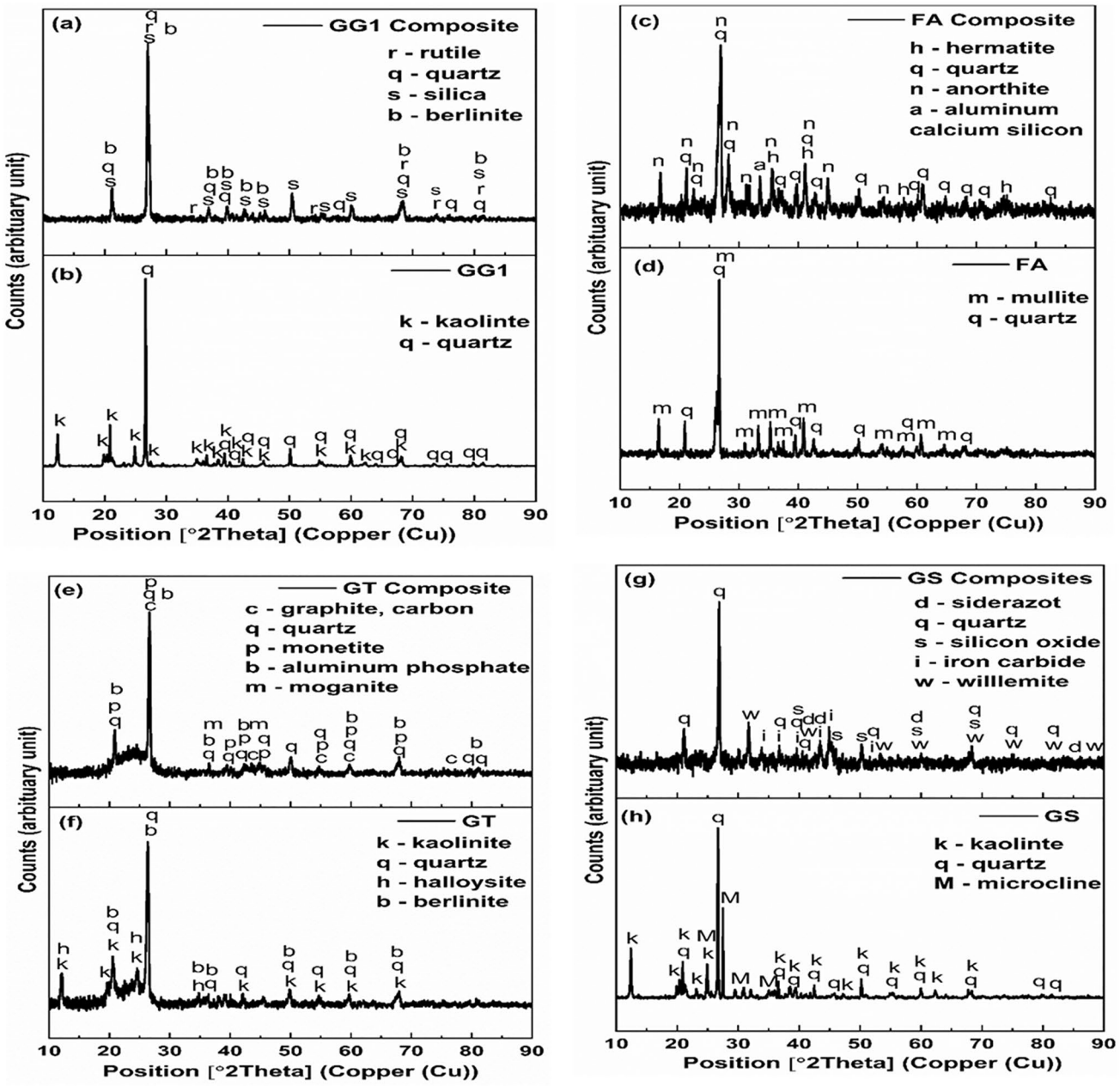

Fig. 4 A comparison of the X-ray diffraction patterns of the coals and coal composites

the GT composite is homogenously darker than the other composites, attributed to the relatively high carbon in the composite. The composites appear smooth; however, at high SEM magnifications, their surfaces are rough. Therefore, to enhance surface smoothness and uniformity, using a polytetrafluoroethylene release film to line the mould in direct contact with the mixture being pressed might be beneficial. Another solution might be to add soluble wetting agents, e.g. water, surfactant, or solvent, to the coal/PCP mixture. The optical microscopic images of fabricated composites (Figs. 6(c, f, i, and l)) show good incorporation of the mixture content and spatial distribution of minerals on the composites' surface. Large quartz grains can be observed on the FA composite, while apatite grains can be seen on the GS composite (Fig. 5b).

Raman analysis

The carbon phase is an important component of carbon-bonded composites. As noted earlier, the mixture of the CBW and the PCP pyrolysed up to 1000 °C could have developed a network of graphene fragments or

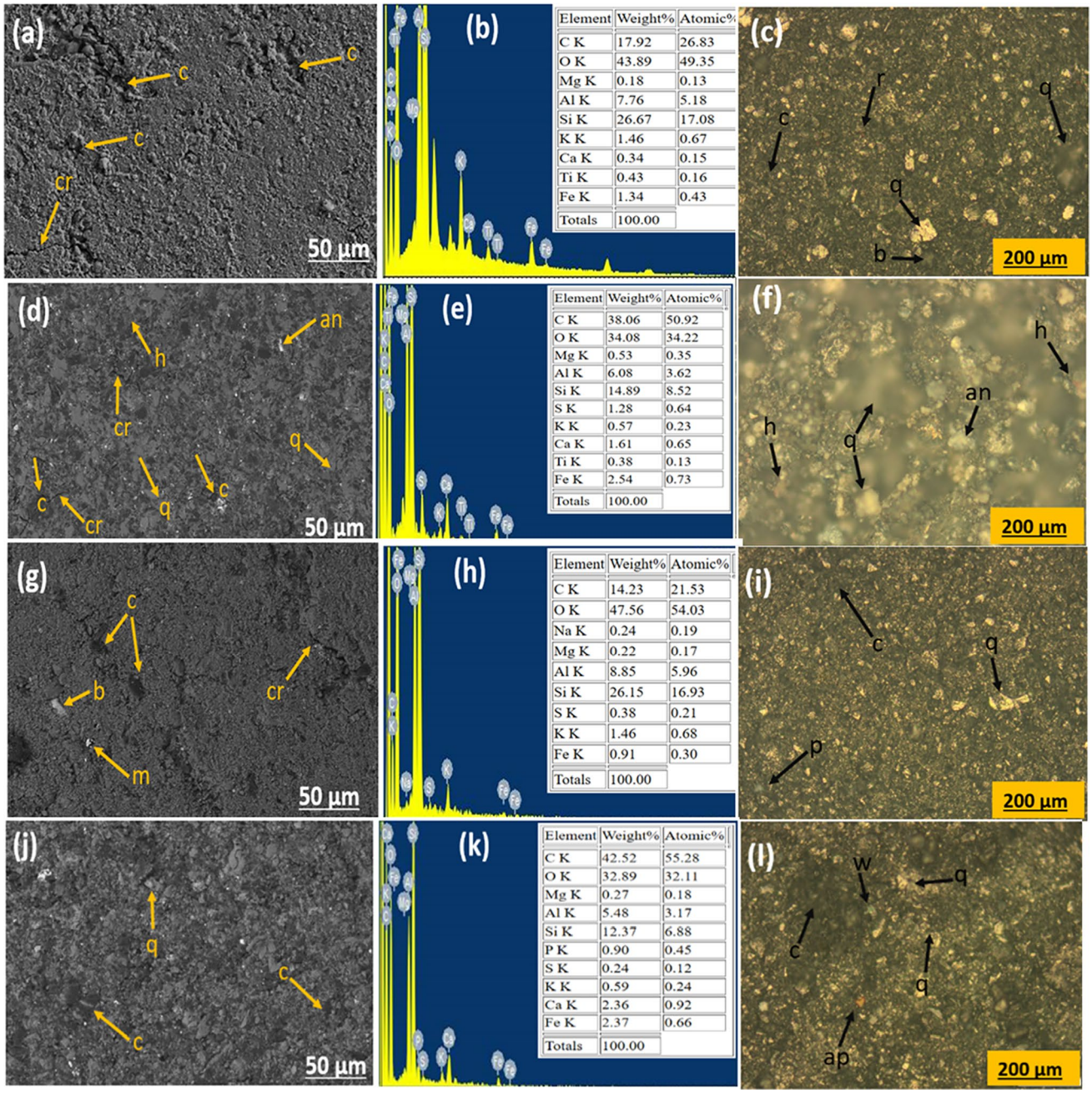

Fig. 5 SEM secondary electron image (**a**); backscattered images (**d**, **g**, **j**); energy-dispersive X-ray spectroscopy (EDS) results (**b**, **e**, **h**, **k**); optical micrographs (**c**, **f**, **i**, **l**) of the produced composites. GG1 (**a**, **b**, **c**); FA (**d**, **e**, **f**); GT (**g**, **h**, **i**); GS (**j**, **k**, **l**) composites (*an* anorthite, *b* aluminium phosphate, *c* carbon, *cr* crack, *h* hematite, *m* monetite, *q* quartz)

nanodomains of graphitic carbon (Sharma 2018; Hill and Easter 2021). Therefore, Raman spectroscopy was used to acquire information pertaining to the carbon structure and the graphitisation degree of the carbon atoms. The Raman spectra of the composites manifest peaks at around 1360 and 1560 cm^{-1}, the typical D-band and G-band in carbon-based materials (Fig. 6). The presence of both bands suggests that the carbon resulting from the pyrolysis of the mixture is in a disorganised state and consists of the infinite repetition of sp^3 and sp^2 hybridised C-C bonds. Broad peaks centred around 2750 cm^{-1} and 3200 cm^{-2}, such as the second-order 2D (or G') and the 2D' bands observed in graphite samples (Ferrari 2007), are more dominant in the Raman spectra of the GG1 and FA composites. In principle, the 2D-band supports the presence of amorphous carbon and is characteristic of turbostratic carbon (Ruz

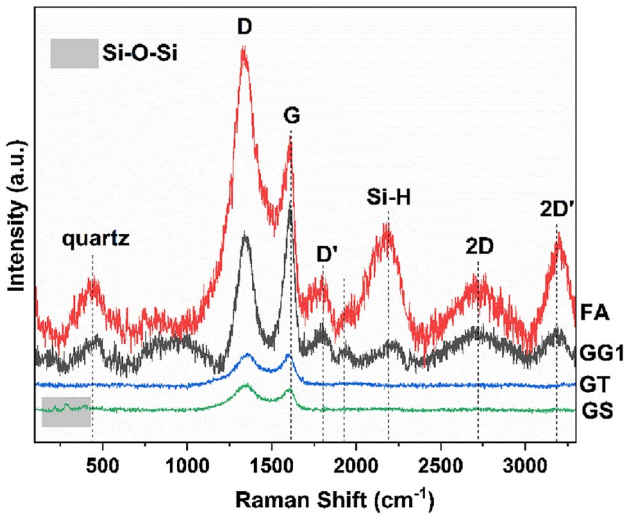

Fig. 6 Raman spectra of the composites

Table 5 Graphitisation indices of the composites

Composites/ Indices	GG1	FA	GT	GS
A_D/A_G	1.45	3.78	2.21	2.90
L_a	3.03	1.16	1.98	1.51

et al. 2016). Also judging by the existence of the 2D peak in the GG1 and FA composites, as speculated earlier, some graphene layers may have formed (Sazali et al. 2016).

The D' peak close to the G-band is usually observed in the nanostructures of disordered carbon materials (Dresselhaus et al. 2010; Pusz et al. 2015), such as those in this study. The emergence of peaks less than 1000 cm^{-1}, such as 445 cm^{-1} associated with quartz and 758 cm^{-1} attributed to the Si-C peak, and the presence of the Si-O-Si bond/vibration can be seen in the spectra of the GG1, FA, and GS composites but surprisingly was not Raman active in the GT composites. A_D/A_G was calculated from the ratio of the areas beneath the D- and G-bands, and the size of carbon crystallites (L_a) was used to quantify the disorder (Table 5). The intensity ratio generally increases with the amount of carbon phase disorder, and the trend follows FA > GS > GT > GG1, meaning that the least graphitic (i.e. highly defective) carbon phases are dominant in the FA composite. The GG1 composite supports the dominance of the graphitic carbon phases (sp^2 C-C bonds) suggesting the formation of fewer defects. A_D/A_G correlates inversely to L_a and agrees with the cluster size of the carbon phase of the composites, FA composites being the least (1.16 nm). As noted earlier, the total carbon of the FA composite (1.46%) was mainly provided by the pyrolysis of the polymer.

Thermal stability/continuous operating temperature of the composites

The thermal stability of the composites was investigated to monitor the quantitative weight change during the thermal degradation of one gram of composites placed in a TGA furnace under different environments (air and oxygen) at a ramp rate of 10 °C/min to 900 °C. The minimum and maximum weight loss rate temperatures and the decomposition temperature at T5% were used to evaluate the thermal stability of the composites (Table 6). Two temperature regions were identified in Fig. 7 where weight loss occurred. Stage 1 weight loss (less than 200 °C) is related to the loss of adsorbed moisture and low molecular weight volatile matter in the case of the GT composite. The weight loss of the GT and GS composites in an air environment (Fig. 7b) around 600 °C (stage 2) was about 9.09% and 4.55%, respectively. Above 600 °C, the GT and GS composites show progressive weight loss of about 14.3% and 14.23%, respectively. The

Table 6 Summary of the thermogravimetric analysis of the composites shown in Fig. 7

Composites	T_1 (°C)	T_2 (°C)	T5% (°C)	Stage 1 weight loss (wt.%)	Stage 2 weight loss (wt.%)	Total weight loss at 900 °C (wt.%)
(a) Oxygen environment (99.5% purity)						
GG1	85.85	650.83	604.14	1.40	9.10	10.50
FA	89.24	633.87	–	0.85	0.41	1.26
GT	104.51	673.97	183	6.36	28.69	35.05
GS	99.21	678.76	593.77	1.54	23.59	25.13
(b) Air environment						
GG1	109.98	683.54	671.57	1.74	8.21	10
FA	90.83	649.23	–	1.12	0.55	1.68
GT	139.11	681.15	191.02	6.23	17.17	23.40
GS	118.56	677.56	609.99	3.19	15.59	18.78

T_1 and T_2 temperature corresponding to the minimum and maximum weight loss rate, *T5%* decomposition temperature at 5% weight loss, *GG1* discard from washing plant, *FA* fly ash, *GT* fine waste, *GS* coal waste from Witbank coalfield

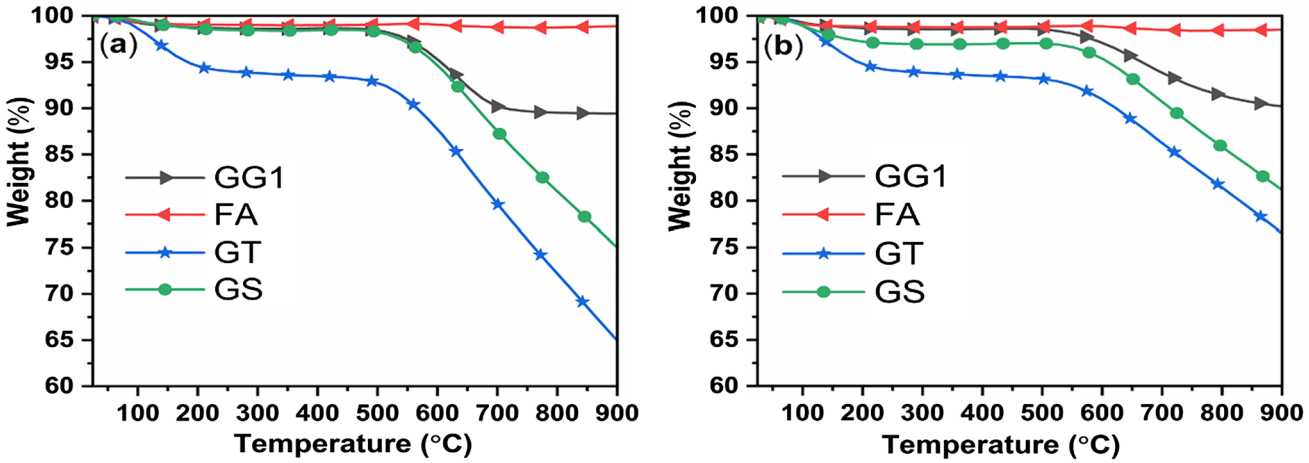

Fig. 7 Thermal analysis (TGA) profiles of the composites under (a) Oxygen (b) Air environment

GT composite displayed the worst thermal stability performance owing to the thermal decomposition of the carbonaceous materials in the composites. In contrast, a small weight change was recorded for the GG1 and FA composites when heated in an oxygen or air environment. FA, being a non-combustible material, produced the most thermally stable composite. This observation is consistent with the XRD results that showed highly stable and high melting point minerals, e.g. quartz, anorthite, and hematite were detected in the FA composite. Besides, the high thermal stability of the GG1 and FA composites suggests they contain a reasonable amount of Si-O bonds and fewer C-C and C-O bonds compared to the GS and GT composites. The bond dissociation energy of the bonds C-C (82.6 kJ/mol) and C-O (85.2 kJ/mol) are low compared to the Si-O bond (108 kJ/mol) (Jones et al. 2013; Stabler et al. 2018).

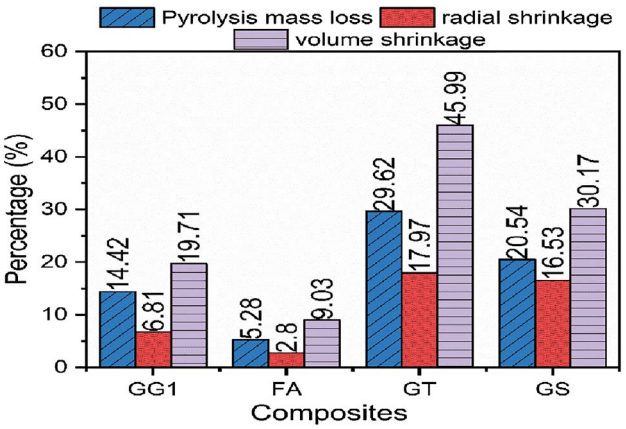

Fig. 8 Average pyrolysis mass loss and shrinkage of the composites

Physical and mechanical analysis of the composites

The difference in the physiochemical structures of the CBW already indicates the possible differences in terms of the properties of the composites. This section discusses the composites' physical properties (bulk density, apparent porosity, pyrolysis shrinkage, and water absorption) and mechanical properties (ultimate compressive stress).

Weight loss and shrinkage during pyrolysis

The shrinkage value after pyrolysis of the cured composites provides useful information on the size of mould or die that would be needed to produce a predetermined composite size. From Fig. 8, the pyrolysis mass loss of the composites is within the range of 5.28 to 29.62%. All the composites retained their shape, but composites produced from the CBW of high inorganic content (GG1 and FA) presented lower shrinkage values. On the contrary, the GT composite recorded substantial weight loss (29.62%), radial shrinkage (17.97%), and volume shrinkage (46%). This was attributed to the nature of the coal and the high volatile matter content (32.7%). This substantial weight/shrinkage loss, which implies a reduction in the free volume of the composites, resulted from a high degree of conversion of the C=C bonds in the coal to C-C bonds (as shown in the FTIR results). For a small-sized sample, the volume shrinkage of the GT and GS composites seems quite high. As such, it could present a challenge if large-size composites were produced. High shrinkage tends to be associated with contraction stress, thermal stress, cracks, deformation, and warping during pyrolysis. In principle, the PCP decomposes during pyrolysis, followed by the release of hydrogen and other species containing carbon and hydrogen that results in mass loss, volume shrinkage, and densification. As a result, the composites contain some ceramic phases homogenously

dispersed in a carbon matrix. Considering that the ratio of the raw materials is 80 wt.% coal and 20 wt.% PCP, it is believed that the shrinkage that occurred is largely dependent on the physicochemical composition of the coal, which, in turn, dictated the degree of conversion of the composites.

Density, water absorption, and apparent porosity of the composites

The bulk density, geometric density, and apparent specific gravity of the composites after the water impregnation stages (five-hour cold test, 24-h cold test, and five-hour boiling test) are displayed in Fig. 9. According to the data, the 24-h cold test and the five-hour boiling test did not significantly increase the density of the composites, demonstrating compactness and micro-cracking of the composites. In general, the bulk density of the composites varied between 1.5 g/cm^3 and 1.9 g/cm^3. The GG1 composite recorded the highest densities while the GT composite had the least overall. The coal from which the GG1 composite was made has the highest ash content, i.e. more inorganic forming minerals. Besides, GG1 is rich in oxygen functional groups, which facilitate curing reactions, as well as physical and chemical interactions with the polymer during pyrolysis. This might have led to the GG1 composite's high density, considering that the FA is also rich in minerals; yet, the FA composite is of lower density than the GG1 composite.

The high shrinkage experienced by the GT composite is due to the nature of the coal and is reflected in the composite's low density. Furthermore, the high volatile matter (32.7%) of GT coal appears to have accelerated degassing and porosity generation within the composite during pyrolysis. Water absorption, i.e. the mass of water absorbed to the mass of the dry composite, provided an indirect measure of porosity and extent of densification. The apparent porosity expresses the volume of open pores of the composites to its exterior volume as a percentage. As expected, the apparent porosity and water absorption follow the same trend, as displayed in Fig. 10. Low water absorption of the GS, FA, and GG1 composites indicates a high volume of impervious

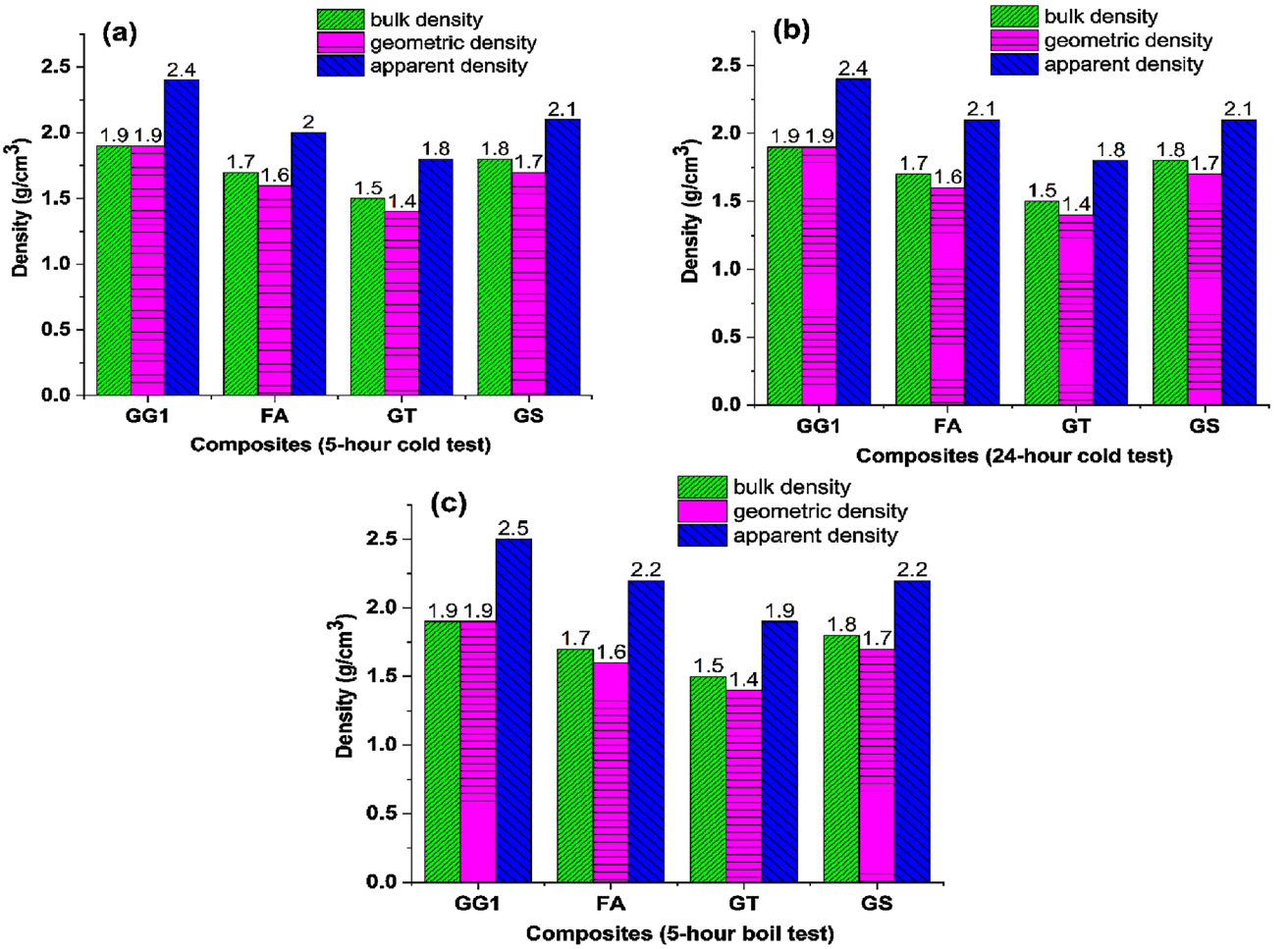

Fig. 9 Bulk, geometric and apparent densities of the composites

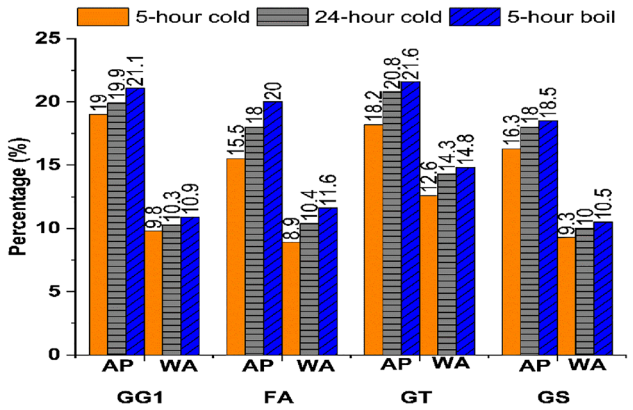

Fig. 10 Average apparent porosity and water absorption of the composites (*AP* average porosity, *WA* water absorption)

pores. These low water absorption composites are essential to resist water intrusion from the natural environment, consequently enhancing their durability. With the water absorption of the composites similar to those of conventional building materials (0 to 25%), these composites may be fabricated into pavement tiles, cladding tiles, bricks, blocks, or roof tiles depending on the application.

Surface property of the composites

Surface property is a critical indicator in the design of coal composites for construction applications as they could impact the durability of composites. In this work, the surface property of the composites was described in terms of the static CA between water and the composite surfaces. The CA was measured from a minimum of four drops on each side of the composite. The CAs of the GT and GS composites with water are less than 90° (Fig. 11), which can be linked to the nonpolar nature of their surface. This observation implies strong interfacial adhesion between the surface of the composites and water. Therefore, the composites have a high tendency to adsorb water. Therefore, they would be highly susceptible to water wetting and may not be useful in applications where interaction with water is needed. In contrast, the CAs of the FA and GG1 composites are greater than 90°, inferring their surfaces are hydrophobic and the force of attraction of water-to-composite is weak. From a practical point of view, these composites are less susceptible to water wetting and penetration, which could cause the composites to deteriorate easily. Apart from being dense and less porous, evidence supporting the FA and GG1 composites maintaining a high CA can be linked to the nonpolar C-H functional groups bound to their surfaces (Gomez-Caturla et al. 2022). As seen from the FTIR spectra (Fig. 11), these hydrophobic functional groups (C-H) are more absorbed in the FA and GG1 composites and are responsible for the weak molecular interaction between water and the composite surface.

Compressive strength performance

The mechanical behaviour of the composites produced was studied using compression tests to investigate the strength of the bonds that connect the atoms and crystals inside the composites. The mechanical properties of the composites in terms of their average ultimate compressive stress are presented in Fig. 12. Given that the various composites offer a difference in their physicochemical properties, the composites produced from the coking coal fines (GT) with 62.66% total carbon and 32% volatile matter, exhibited the lowest resistance to compression (278 MPa). Due to the nature of this coal, it could be postulated that at lower temperatures,

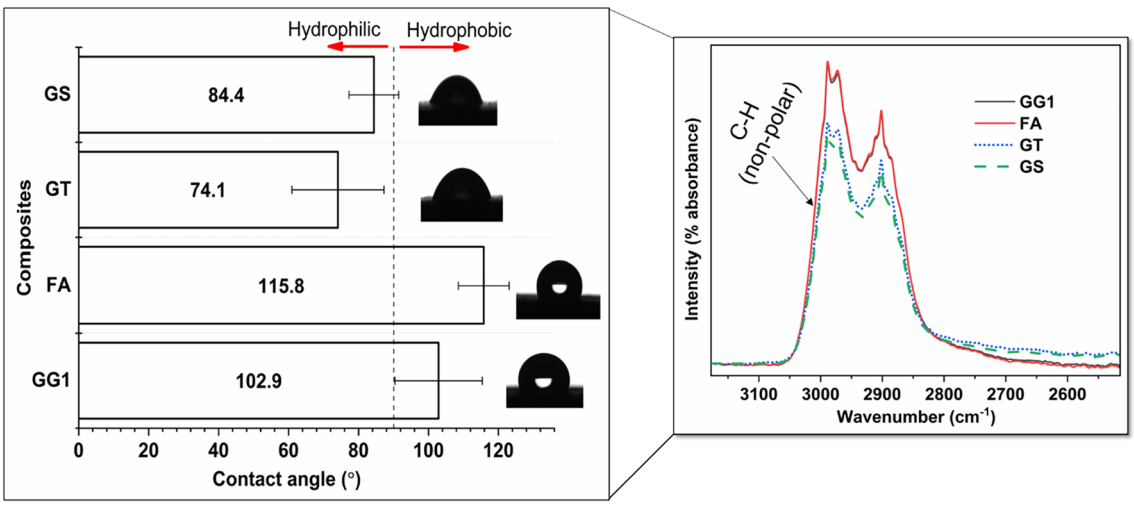

Fig. 11 The water contact angle of the composites measured by the sessile drop method and FTIR of the nonpolar C-H group (right)

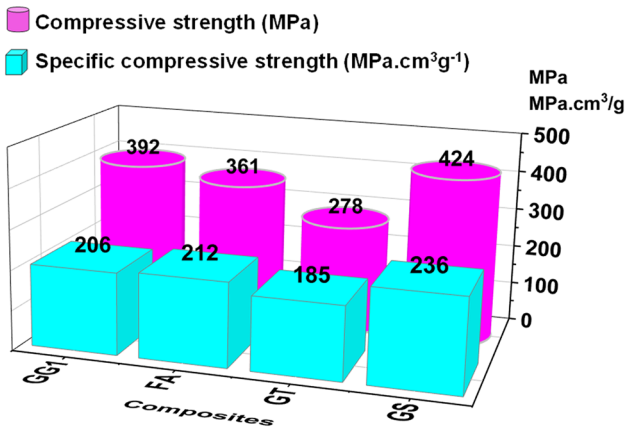

Fig. 12 Average ultimate compressive stress and specific compressive strength of the composites

GT swelled and experienced better heat transfer with the polymer than the other wastes. Hence, by pyrolysing the composite up to 1000 °C, it is likely that char-like composites with large pores could have formed. These pores might have constituted stress concentrators under load that led to the low mechanical stability of the composites.

The high compressive strength of the GS, GG1, and FA composites can be linked to their high bulk densities. Increased strength is known to come with increased density (Hill and Easter 2021). Besides, the formation of the anorthite phase in the FA composite may have contributed to its strength (Kairakbaev et al. 2017). Comparing the strength of the GG1, FA, and GS composites, GS displays the highest strength while FA has the lowest. The lack of reactive sites (inertness of their surfaces) in FA led to weak interactions with the PCP during pyrolysis, consequently lowering the strength. The use of silane coupling agents can provide adequate reaction sites that would significantly enhance the reactions during pyrolysis but with an additional cost. Interestingly, the mechanical response of the GS composite is the best. This suggests that a certain limit of carbon in the CBW may seem sufficient to increase the bonding capacity of the mix and a relatively high carbon content of the CBW could compromise the strength of the final composites. Therefore, it can be postulated that for a relatively high carbon content CBW and depending on the nature of the coal, the bond strength of the mixture pyrolysed up to 1000 °C would reduce sharply. Comparatively, in terms of their specific compressive strength (MPa.cm^3/g), i.e. the strength-to-density ratio, GS recorded the highest, suggesting that the GS composite might be more advantageous for lightweight and high-performance construction material (Ming et al. 2019).

The comparison of the physicomechanical performance of the composites produced in this study to other composites for building applications in the literature is listed in Table 7. The radar chart (Fig. 13a, b, c) illustrates the correlation of the hydrogen/carbon ratio, ash content, and volatile matter of CBW on the key performance properties of the coal/PSO composites. It can be seen that higher H/C ratio CBW (GG1) produced the best quality composites in terms of water absorption, compressive strength, and thermal stability. This is because of the many hydrogen bonds contained in the molecules of this coal waste that enabled it bind effectively with the polymer during pyrolysis (Hu et al. 2017; Hill and Easter 2019). On the other hand, a clear distinction in the low thermal weight loss and carbon content of the composites produced from high-ash wastes (GG1 and FA)

Table 7 The physicomechanical performance of the composites produced in this study compared to other composites for building applications in the literature

Materials	LS (%)	BD (g/cm^3)	WA (%)	AP (%)	CS/FS (MPa)	References
CFA/NaOH/ feldspar/HPC	14.94	–	0.30	0.62	–/40.25	Luo et al. (2019)
Core sand/clay/water	1.8–3.1	–	5.9–10	–	–	Alonso-Santurde et al. (2012)
Clay/wood pulp/WS/FS	–	< 2	10–16	29–39	–/ < 8	Quijorna et al. (2012)
RM/α-Al_2O_3/γ-Al_2O_3/ρ-$Al(OH)_3$	-	1.83–1.94	7.37	18.56	–/185.46	Wang et al., (2020)
CBW/PCP(XMAT)	~20–~27	1.69–1.77	1.94–10.1	3.44–17.1	84–209/28–35	Eterigho-Ikelegbe et al. (2021b)
CBW/clay/water	–	1.54–1.77	19.4–27.7		18.6–25.8/1.6–2.1	Gökçe et al. (2018)
CBW/clay/water	–	1.5–1.9	20.5–29.5	31.2/48.9	7–21.3/–	Bonczyk and Rubin (2022)
CBW/PCP(XMAT)	18–19.4	1.46–1.7	–	–	–/35–125	Hill and Easter (2019)
CBW/shale/IOT/ SS/water	8.3	1.64	17.5	–	14.24/–	Luo et al. (2020)
CBW/SPR-212	2.8–16.53	1.5–1.9	8.9–14.8	15.5–21.6	278–424/–	Our work

LS linear shrinkage, *BD* bulk density, *WA* water absorption, *AP* apparent porosity, *CS* compressive strength, *FS* flexural strength, *CFA* coal fly ash, *HPC* high plastic clay, *WS* waelz slag, *FS* foundry sand, *RD* red mud, *CBW* coal-based waste, *PCP* preceramic polymer, *IOT* iron ore tailings, *SS* sewage sludge

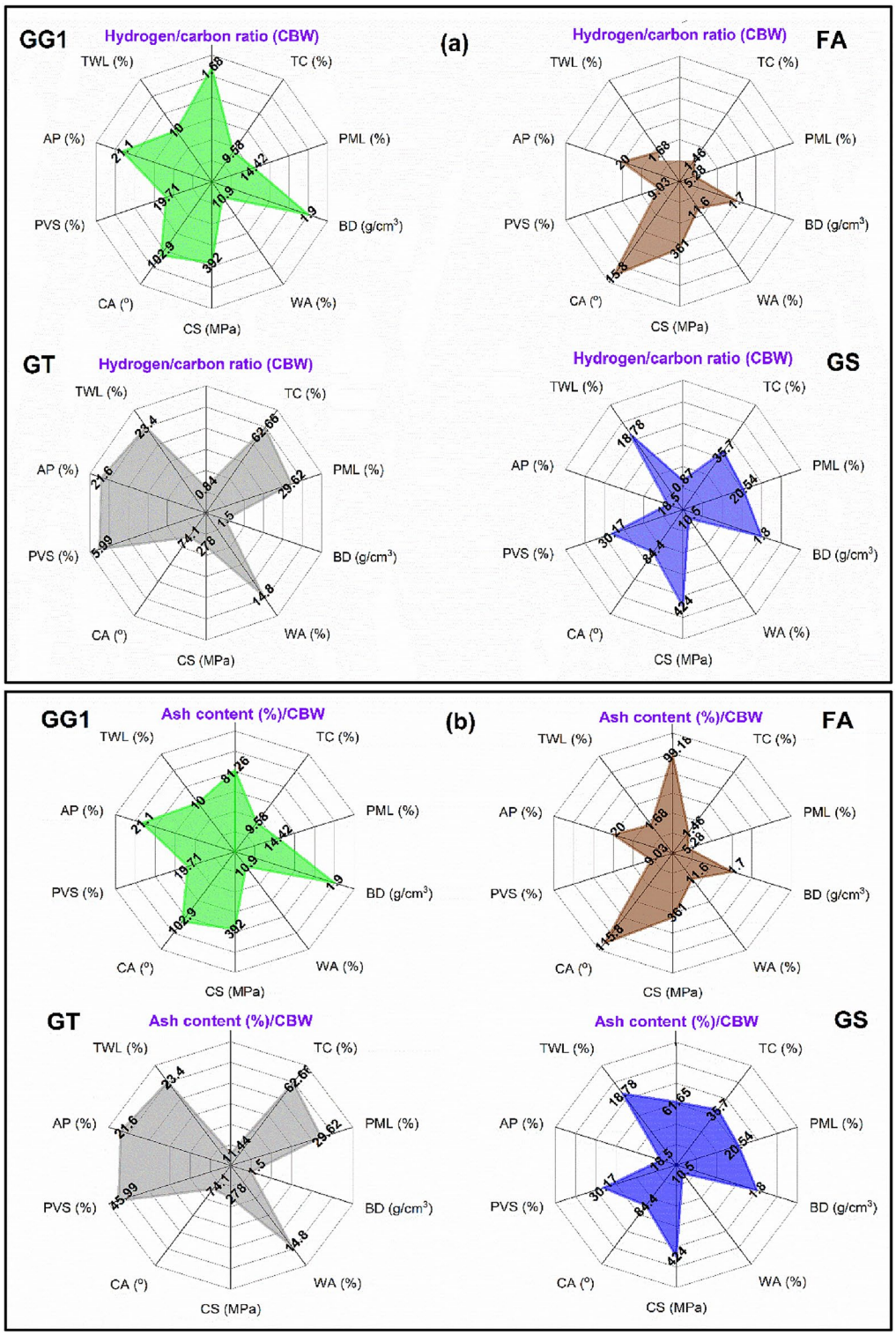

Fig. 13 The correlation between **a** hydrogen/carbon ratio **b** ash content **c** volatile matter of CBW on the key performance properties of the composites (*TC* total carbon, *PML* pyrolysis mass loss, *BD* bulk density, *WA* water absorption, *CS* compressive strength, *CA* contact angle, *PVS* pyrolysis volume shrinkage, *AP* apparent porosity, *TWL* thermal weight loss, *GG1* discard from washing plant, *FA* fly ash, *GT* fine waste, *GS* coal waste from Witbank coalfield)

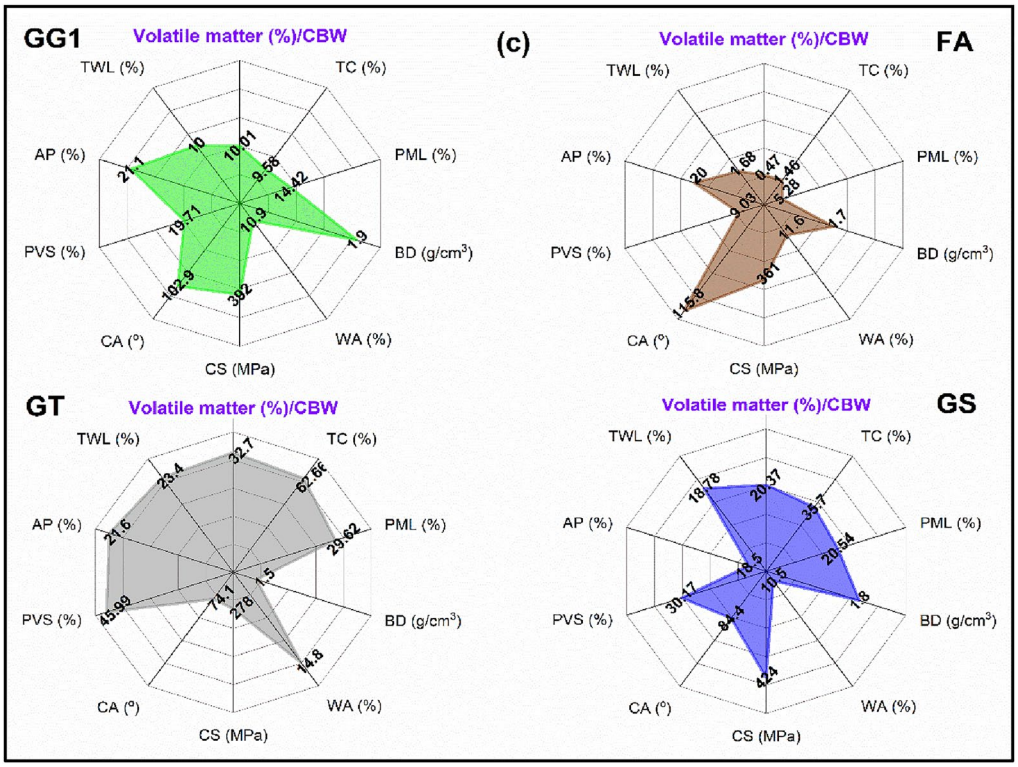

Fig. 13 (continued)

is due to the presence of many non-combustible materials in these wastes. Finally, high volatile CBW (GT) yielded composites with the least desired properties overall for building applications (lowest compression strength, highest water absorption, and lowest water contact angle).

Conclusion

Processing coal-based waste into high-value composites seems like a good way to manage and transform this problematic waste. The variation in the physicochemical properties of coal-based waste on the resultant composites using the poly(organo)siloxane SPR-212 as the ceramic-forming binder was studied. The GT fines used in this study contain the highest percentage of volatile matter and total carbon. As a result, the GT composite displayed the poorest qualities based on the properties evaluated. The relatively high total carbon (36%) in the GT and GS composites increased their susceptibility to heat; hence, their dramatic degradation above 600 °C. Furthermore, the evidence appears to suggest that the reactive functional groups present in GG1 waste promoted the reactivity of GG1 with SPR-212. As a result, high-quality GG1 composites were produced compared to the other composites. Despite its chemical inertness, FA yielded composites of interesting properties. The water absorption of the coal composites produced in this study is in the range of 0 and 25%, and their ultimate compressive stress was up to 420 MPa. Based on the promising results documented in this study, these composites may be designed into roofing tiles, blocks, bricks, or cladding tiles for building applications. However, further development in terms of optimising the process conditions and upscaling the process to produce technical-size coal composites are of great interest for the application of these advanced and sustainable building materials.

Acknowledgements Orevaoghene Eterigho-Ikelegbe thankfully acknowledges the financial support received from the Department of Science and Innovation National Research Foundation (DSI–NRF) South African Research Chairs Initiative (SARChI) Clean Coal Technology Grant (Grant Number: 86421). The composites were fabricated in the Fachbereich Materialwissenschaft within the Technische Universität Darmstadt, Germany and supported by the German Academic Exchange Service (DAAD) under the short-term research grants (57552337). The authors wish to thank Petra Dinham for obtaining SEM images and Professor Rudolph Erasmus for obtaining Raman spectra. The authors would like to acknowledge the laboratory assistant provided by Mingxing Li.

Author contributions OE-I contributed to methodology, investigation, formal analysis, writing—original draft, and writing—review and editing. ER III contributed to writing—review and editing. HH contributed to writing—review and editing. RR contributed to resources, supervision, and writing—review and editing. SB contributed to

conceptualisation, funding acquisition, resources, supervision, and writing—review and editing.

Funding Open access funding provided by University of the Witwatersrand.

Data availability Enquiries about data availability should be directed to the authors.

Declarations

Conflict of interest The authors have no relevant financial or non-financial interests to disclose.

References

Abdulsalam J, Mulopo J, Bada S, Oboirien B (2020) Natural gas storage properties of adsorbents synthesised from three different coal waste in South Africa. Fuel 267:117157. https://doi.org/10.1016/j.fuel.2020.117157

Al-Majali YA, Chirume CT, Marcum EP, Daramola DA, Kappagantula KS, Trembly JP (2019) Coal-filler-based thermoplastic composites as construction materials: a new sustainable end-use application. ACS Susta Chem Eng 7:16870–16878. https://doi.org/10.1021/acssuschemeng.9b04453

Alonso-Santurde R, Coz A, Viguri JR, Andrés A (2012) Recycling of foundry by-products in the ceramic industry: green and core sand in clay bricks. Constr Build Mater 27:97–106. https://doi.org/10.1016/j.conbuildmat.2011.08.022

ASTM C373, 2018a. Standard test methods for determination of water absorption and associated properties by vacuum method for pressed ceramic tiles and glass tiles and boil method for extruded ceramic tiles and non-tile fired ceramic whiteware products

ASTM C67, 2010. Standard test methods for sampling and testing brick and structural clay tile

ASTM D5142, 2009. Standard test methods for proximate analysis of the analysis sample of coal and coke by instrumental procedures.

Bai YF, Cao XX, Xu ML, He XF, Cai GH (2019) Coal Powder and Ethylene-Propylene-Diene Monomer Reinforced Hybrid Polypropylene Composites. Mater Sci Forum 956:192–200. https://doi.org/10.4028/www.scientific.net/MSF.956.192

Blissett RS, Rowson NA (2012) A review of the multi-component utilisation of coal fly ash. Fuel 97:1–23. https://doi.org/10.1016/j.fuel.2012.03.024

Bonczyk M, Rubin J (2022) The application of coal mining waste to the production of construction ceramics: radiological and mechanical aspects. Mater Constr 72:e300–e300. https://doi.org/10.3989/mc.2022.01822

Černý M, Chlup Z, Strachota A, Halasová M, Rýglová Š, Schweigstillová J, Svítilová J, Havelcová M (2015) Changes in structure and in mechanical properties during the pyrolysis conversion of crosslinked polymethylsiloxane and polymethylphenylsiloxane resins to silicon oxycarbide glass. Ceram Int 41:6237–6247. https://doi.org/10.1016/j.ceramint.2015.01.034

Colombo P, Mera G, Riedel R, Sorarù GD (2010) Polymer-Derived Ceramics: 40 Years of Research and Innovation in Advanced Ceramics. In: Ceramics Science and Technology. John Wiley & Sons, Ltd, pp. 245–320. https://doi.org/10.1002/9783527631971.ch07

Dresselhaus MS, Jorio A, Souza Filho AG, Saito R (2010) Defect characterization in graphene and carbon nanotubes using Raman spectroscopy. Philos Trans R Soc Math Phys Eng Sci 368:5355–5377. https://doi.org/10.1098/rsta.2010.0213

Eckel ZC, Zhou C, Martin JH, Jacobsen AJ, Carter WB, Schaedler TA (2016) Additive manufacturing of polymer-derived ceramics. Science 351:58–62. https://doi.org/10.1126/science.aad2688

Eterigho-Ikelegbe O, Harrar H, Bada S (2021a) Rare earth elements from coal and coal discard —a review. Miner Eng 173:107187. https://doi.org/10.1016/j.mineng.2021.107187

Eterigho-Ikelegbe O, Trammell R, Bada S (2021b) Preparation and characterization of ceramic composites from South Africa coal discard. Constr Build Mater 302:124164. https://doi.org/10.1016/j.conbuildmat.2021.124164

Eterigho-Ikelegbe O, Yoro KO, Bada S (2021c) Coal as a filler in polymer composites: a review. Resour Conserv Recycl 174:105756. https://doi.org/10.1016/j.resconrec.2021.105756

Eterigho-Ikelegbe O, Trammell R, Bada SO (2022) Novel ceramic composites produced from coal discards with potential application in the building and construction sectors. J South Afr Inst Min Met 122:421–428. https://doi.org/10.17159/2411-9717/2001/2022

Fecko P, Tora B, Tod M (2013) Coal waste: handling, pollution impacts and utilization. In: Osborne D (ed) The Coal Handbook: Towards Cleaner Production, Woodhead Publishing Series in Energy. Woodhead Publishing, Cambridge, pp 63–84. https://doi.org/10.1533/9781782421177.1.63

Ferrari AC (2007) Raman spectroscopy of graphene and graphite: Disorder, electron–phonon coupling, doping and nonadiabatic effects. Solid State Commun Explor Graphene 143:47–57. https://doi.org/10.1016/j.ssc.2007.03.052

Ferraro JR, Basile LJ (2012) Fourier transform infrared spectra: applications to chemical systems. Academic Press, Cambridge

Gökçe M, Akçaözoğlu S, Sinani B (2018) Investigation of Production of Brick with Waste Coal Powder Additive. In: UBT International Conference

Gomez-Caturla J, Balart R, Ivorra-Martinez J, Garcia-Garcia D, Dominici F, Puglia D, Torre L (2022) Biopolypropylene-based wood plastic composites reinforced with mango peel flour and compatibilized with an environmentally friendly copolymer from itaconic acid. ACS Appl Polym Mater 4:4398–4410. https://doi.org/10.1021/acsapm.2c00373

Greil P (1995) Active-Filler-Controlled Pyrolysis of Preceramic Polymers. J Am Ceram Soc 78:835–848. https://doi.org/10.1111/j.1151-2916.1995.tb08404.x

Gumula T, Paluszkiewicz C, Blazewicz S (2009) Study on thermal decomposition processes of polysiloxane polymers—From polymer to nanosized silicon carbide. J Anal Appl Pyrol 86:375–380

Haibin L, Zhenling L (2010) Recycling utilization patterns of coal mining waste in China. Resour Conserv Recycl 54:1331–1340. https://doi.org/10.1016/j.resconrec.2010.05.005

Harrar H, Eterigho-Ikelegbe O, Modiga A, Bada S (2022) Mineralogy and distribution of rare earth elements in the Waterberg coalfield high ash coals. Miner Eng 183:107611. https://doi.org/10.1016/j.mineng.2022.107611

Haywood LK, de Wet B, de Lange W, Oelofse S (2019) Legislative challenges hindering mine waste being reused and repurposed

in South Africa. Extr Ind Soc 6:1079–1085. https://doi.org/10.1016/j.exis.2019.10.008
Hill A, Easter W (2019) Carbon Ceramic Composites and Methods (Google Patents), Patent No: US20190292441A1
Hill A, Easter W (2021) Carbon ceramic composites and methods (Google Patents), Patent No: US10988680B2
Hill A, Sherwood W, Trammell R, Easter W (2022) High strength, tough, coal and coal by-product based composite ceramics (Google Patents), Patent No: US20220144706A1
Hossain MdU, Ng ST, Antwi-Afari P, Amor B (2020) Circular economy and the construction industry: Existing trends, challenges and prospective framework for sustainable construction. Renew Sustain Energy Rev 130:109948. https://doi.org/10.1016/j.rser.2020.109948
Hu LL (2016) Coal gangue and its application research in building materials. Mater Sci Forum 873:96–104. https://doi.org/10.4028/www.scientific.net/MSF.873.96
Hu G, Bian Z, Xue R, Huang W, Komarneni S (2017) Polymer-coal composite as a novel plastic material. Mater Lett 197:31–34. https://doi.org/10.1016/j.matlet.2017.03.148
Ionescu E, Kleebe H-J, Riedel R (2012) Silicon-containing polymer -derived ceramic nanocomposites (PDC-NCs): preparative approaches and properties. Chem Soc Rev 41:5032–5052. https://doi.org/10.1039/C2CS15319J
Isaac K, Bada SO (2020) The co-combustion performance and reaction kinetics of refuse derived fuels with South African high ash coal. Heliyon 6:e03309. https://doi.org/10.1016/j.heliyon.2020.e03309
ISO 13909-1, (2018b) Hard coal and coke - Mechanical sampling - Part 1: General introduction
ISO/TS 12902, 2001. Solid mineral fuels - Determination of total carbon, hydrogen, and nitrogen - Instrumental methods.
Jones RG, Ando W, Chojnowski J (2013) Silicon-Containing Polymers: The Science and Technology of Their Synthesis and Applications. Springer, Berlin
Kairakbaev AK, Abdrakhimova ES, Abdrakhimov VZ (2017) Effect of different coal-enrichment wastes on the physical and mechanical properties and phase composition of heat-insulation materials. Glass Ceram 74:55–59. https://doi.org/10.1007/s10717-017-9928-x
Khare P, Baruah BP (2014) Thermogravimetric analysis of perhydrous Indian coals. Energy Sour Part A Recover Util Environ Eff 36:774–782. https://doi.org/10.1080/15567036.2010.547919
Li D, Wu D, Xu F, Lai J, Shao L (2018) Literature overview of Chinese research in the field of better coal utilization. J Clean Prod 185:959–980. https://doi.org/10.1016/j.jclepro.2018.02.216
Liew L, Zhang W, An L, Shah S, Luo R, Liu Y, Cross T, Dunn ML, Bright V, Daily JW (2000) Ceramic MEMS. Am Ceram Soc Bull 80:25
Liu X, Wang Y, Zhan L (2018) Carbon foams prepared from coal tar pitch for building thermal insulation material with low cost. Chin J Chem Eng 26:415–420. https://doi.org/10.1016/j.cjche.2017.04.012
Luo Y, Wu Y, Ma S, Zheng S, Chu PK (2019) An eco-friendly and cleaner process for preparing architectural ceramics from coal fly ash: Pre-activation of coal fly ash by a mechanochemical method. J Clean Prod 214:419–428. https://doi.org/10.1016/j.jclepro.2018.12.292
Luo L, Li K, Fu W, Liu C, Yang S (2020) Preparation, characteristics and mechanisms of the composite sintered bricks produced from shale, sewage sludge, coal gangue powder and iron ore tailings. Constr Build Mater 232:117250. https://doi.org/10.1016/j.conbuildmat.2019.117250
Mbedzi MD, van der Poll HM, van der Poll JA (2020) Enhancing a decision-making framework to address environmental impacts of the South African coalmining industry. Energies 13:4897. https://doi.org/10.3390/en13184897
Ming LY, Sandu AV, Yong HC, Tajunnisa Y, Azzahran SF, Bayuji R, Loong FK (2019) Compressive strength and thermal conductivity of fly ash geopolymer concrete incorporated with lightweight aggregate, expanded clay aggregate and foaming agent. Rev Chim 70(11):4021–4028
Morgan DR, Wade FH (2021) Coal based silicon carbide foam (Google Patents), Patent No: US20210395096A1.
O'Gorman JV, Walker PL (1973) Thermal behaviour of mineral fractions separated from selected American coals. Fuel 52:71–79. https://doi.org/10.1016/0016-2361(73)90016-1
OECD (2015) Material Resources, Productivity and the Environment. Organisation for Economic Co-operation and Development, Paris
Pacheco-Torgal F, Labrincha JA (2013) The future of construction materials research and the seventh UN millennium development goal: a few insights. Constr Build Mater Special Sect Recycl Wastes Use Constr Mater 40:729–737. https://doi.org/10.1016/j.conbuildmat.2012.11.007
Phillips LN, Kappagantula KS, Trembly JP (2019) Mechanical performance of thermoplastic composites using bituminous coal as filler: Study of a potentially sustainable end-use application for Appalachian coal. Polym Compos 40:591–599. https://doi.org/10.1002/pc.24696
Pusz S, Szeluga U, Nagel B, Czajkowska S, Galina H, Strzezik J (2015) The influence of structural order of anthracite fillers on the curing behavior, morphology, and dynamic mechanical thermal properties of epoxy composites. Polym Compos 36:336–347. https://doi.org/10.1002/pc.22948
Quijorna N, Coz A, Andres A, Cheeseman C (2012) Recycling of Waelz slag and waste foundry sand in red clay bricks. Resour Conserv Recycl 65:1–10. https://doi.org/10.1016/j.resconrec.2012.05.004
Rautenbach R, Matjie RH, Strydom CA, Bunt JR, Ward CR, French D, Van Alphen C (2020) Evaluation of mineral matter transformations in low-temperature ashes of South African coal feedstock samples and their density separated cuts using high-temperature X-ray diffraction. Int J Coal Prep Util 40:320–347. https://doi.org/10.1080/19392699.2019.1677629
Ruz P, Banerjee S, Pandey M, Sudarsan V, Sastry PU, Kshirsagar RJ (2016) Structural evolution of turbostratic carbon: Implications in H2 storage. Solid State Sci 62:105–111. https://doi.org/10.1016/j.solidstatesciences.2016.10.017
Sazali NES, Deraman M, Omar R, Othman MAR, Suleman M, Shamsudin SA, Tajuddin NSM, Hanappi MFYM, Hamdan E, Nor NSM, Basri NH (2016) Preparation and structural characterization of turbostratic-carbon/graphene derived from amylose film. AIP Conf Proc 1784:040009. https://doi.org/10.1063/1.4966795
Sharma S (2018) Glassy carbon: a promising material for micro- and nanomanufacturing. Materials 11:1857. https://doi.org/10.3390/ma11101857
Sherwood W, Hill A, Nameni G, Easter W (2021) Composite tile and method of manufacture
Solomon PR (1981) Coal Structure and Thermal Decomposition, in: New Approaches in Coal Chemistry, ACS Symposium Series. American Chemical Society, pp. 61–71. https://doi.org/10.1021/bk-1981-0169.ch004
Song D, Yang C, Zhang X, Su X, Zhang X (2011) Structure of the organic crystallite unit in coal as determined by X-ray diffraction. Min Sci Technol (china) 21:667–671. https://doi.org/10.1016/j.mstc.2011.10.004
Stabler C, Ionescu E, Graczyk-Zajac M, Gonzalo-Juan I, Riedel R (2018) Silicon oxycarbide glasses and glass-ceramics: "All-Rounder" materials for advanced structural and functional applications. J Am Ceram Soc 101:4817–4856. https://doi.org/10.1111/jace.15932

Stolboushkin A, Yu Ivanov AI, Fomina OA (2016) Use of Coal-Mining and Processing Wastes in Production of Bricks and Fuel for Their Burning. Procedia Engineering. In: 2nd International Conference on Industrial Engineering (ICIE-2016) 150, 1496–1502. https://doi.org/10.1016/j.proeng.2016.07.089

Taha Y, Benzaazoua M, Hakkou R, Mansori M (2017) Coal mine wastes recycling for coal recovery and eco-friendly bricks production. Miner Eng Sustain Miner 107:123–138. https://doi.org/10.1016/j.mineng.2016.09.001

Tambwe O, Kotsiopoulos A, Harrison STL (2020) Desulphurising high sulphur coal discards using an accelerated heap leach approach. Hydrometallurgy 197:105472. https://doi.org/10.1016/j.hydromet.2020.105472

Tan J, Cheng H, Wei L, Wei C, Xing Y, Gui X (2019) Using low-rank coal slime as an eco-friendly replacement for carbon black filler in styrene butadiene rubber. J Clean Prod 234:949–960. https://doi.org/10.1016/j.jclepro.2019.06.221

van der Merwe EM, Prinsloo LC, Mathebula CL, Swart HC, Coetsee E, Doucet FJ (2014) Surface and bulk characterization of an ultrafine South African coal fly ash with reference to polymer applications. Appl Surf Sci 317:73–83. https://doi.org/10.1016/j.apsusc.2014.08.080

van Niekerk D (2008) Structural elucidation, molecular representation and solvent interactions of vitrinite-rich and inertinite-rich South African coals. Ph.D. Thesis

Vasić MV, Goel G, Vasić M, Radojević Z (2021) Recycling of waste coal dust for the energy-efficient fabrication of bricks: a laboratory to industrial-scale study. Environ Technol Innov 21:101350. https://doi.org/10.1016/j.eti.2020.101350

Wang GH, Zhou AN (2011) Effect of coal structure on mechanical and thermal properties of coal filled soy protein composites. Adv Mater Res 236–238:288–291. https://doi.org/10.4028/www.scientific.net/AMR.236-238.288

Wang W, Sun K, Liu H (2020) Effects of different aluminum sources on morphologies and properties of ceramic floor tiles from red mud. Constr Build Mater 241:118119. https://doi.org/10.1016/j.conbuildmat.2020.118119

Wen Q, Qu F, Yu Z, Graczyk-Zajac M, Xiong X, Riedel R (2022) Si-based polymer-derived ceramics for energy conversion and storage. J Adv Ceram 11:197–246. https://doi.org/10.1007/s40145-021-0562-2

Xifan W 2019. Photoinduced thiol-ene click chemistry assisted additive manufacturing and freeze casting of polymer-derived ceramics. Universitätsverlag der TU Berlin

Xu H, Song W, Cao W, Shao G, Lu H, Yang D, Chen D, Zhang R (2017) Utilization of coal gangue for the production of brick. J Mater Cycles Waste Manag 19:1270–1278. https://doi.org/10.1007/s10163-016-0521-0

Yao ZT, Xia MS, Sarker PK, Chen T (2014) A review of the alumina recovery from coal fly ash, with a focus in China. Fuel 120:74–85. https://doi.org/10.1016/j.fuel.2013.12.003

Yao ZT, Ji XS, Sarker PK, Tang JH, Ge LQ, Xia MS, Xi YQ (2015) A comprehensive review on the applications of coal fly ash. Earth Sci Rev 141:105–121. https://doi.org/10.1016/j.earscirev.2014.11.016

Yuan Q, Robert D, Mohajerani A, Tran P, Pramanik BK (2022) Utilisation of waste-to-energy fly ash in ceramic tiles. Constr Build Mater 347:128475. https://doi.org/10.1016/j.conbuildmat.2022.128475

Zhang Y, Song H, Liu Q, Zhang S, Zhang Y (2017) Dynamic mechanical property of kaolinite/styrene-butadiene rubber composites. Mech Mater Sci Eng J. https://doi.org/10.2412/mmse.61.54.732

Zhao B (2012) Environmental assessment of Durban Navigation Colliery discard dumps in the Klip River coalfield, Kwazulu-Natal Province of South Africa. Environ Earth Sci 67:743–757. https://doi.org/10.1007/s12665-012-1533-2